

Solar jet-coronal hole collision and a related coronal mass ejection

Ruisheng Zheng, Yao Chen, Guohui Du, and Chuanyang Li

*Shandong Provincial Key Laboratory of Optical Astronomy and Solar-Terrestrial Environment,
and Institute of Space Sciences, Shandong University, 264209, Weihai, China;
ruishengzheng@sdu.edu.cn*

ABSTRACT

Jets are defined as impulsive, well-collimated upflows, occurring in different layers of the solar atmosphere with different scales. Their relationship with coronal mass ejections (CMEs), another type of solar impulsive events, remains elusive. Using the high-quality imaging data of AIA/SDO, here we show a well-observed coronal jet event, in which part of the jets, with the embedding coronal loops, runs into a nearby coronal hole (CH) and gets bounced towards the opposite direction. This is evidenced by the flat-shape of the jet front during its interaction with the CH and the V-shaped feature in the time-slice plot of the interaction region. About a half-hour later, a CME initially with a narrow and jet-like front is observed by the LASCO C2 coronagraph, propagating along the direction of the post-collision jet. We also observe some 304 Å dark material flowing from the jet-CH interaction region towards the CME. We thus suggest that the jet and the CME are physically connected, with the jet-CH collision and the large-scale magnetic topology of the CH being important to define the eventual propagating direction of this particular jet-CME eruption.

Subject headings: Sun: activity — Sun: corona — Sun: coronal mass ejections (CMEs)

1. Introduction

Solar coronal jets, first observed in X-rays with the Soft X-ray Telescope (XRT, Tsuneta et al. 1991) on board the Yohkoh satellite, represent a group of impulsive events characterized by well-collimated upflows with different scales developing in different layers of the solar atmosphere (e.g., Shibata et al. 1992; Savcheva et al. 2007; Chen et al. 2012). They are generally believed to be energized by magnetic reconnection, often associated with an inverse Y-shaped, anemone-like configuration involving open field lines in coronal holes (CHs) or open-like large-scale closed loops extending from an active region (Shibata et al. 1992, 2007; Schmieder et al. 1995; Rachmeler et al. 2010; Pariat et al. 2009, 2015). These open or open-like field lines are important in collimating jets.

Coronal mass ejections (CMEs) are another type of impulsive energy release events in the solar atmosphere, with a much larger scale and stronger impact on nearby coronal structures such as streamers and CHs. There exist a number of studies examining the strong CME disturbance to coronal streamers (e.g., Hundhausen et al. 1987; Sheeley et al. 2000; Tripathi & Raouafi 2007; Chen et al. 2010). In the meantime, both streamers and CHs have been suggested to have effects on the propagating direction of CMEs, a crucial factor determining the CME geo-effectiveness. For instance, Gopalswamy et al. (2009) reported events with sources very close to the solar disk center that are unexpectedly *NOT* associated with interplanetary CMEs (yet accompanied by interplanetary shocks), and they attributed this to possible interaction and further deflection of CMEs by nearby CH(s). Nevertheless, a direct observation of this CME-CH interaction process remains absent. Neither do we know how and where the deflection takes place.

While both jet and CME represent impulsive ejection of plasmas to upper levels of the solar atmosphere, their relationship remains obscure. Can a relatively large-and-fast jet drive a CME or can the CME actually trigger some jets, by, for example, opening initially-closed magnetic field? Different scenarios have been developed (e.g., Pariat et al. 2009, 2015), and actual answers may differ to different event, depending on specific circumstances¹. It is also very interesting to ask, considering the above-mentioned possibility of strong CME-CH interaction, can a jet, if moving along large-scale active region loops, actually interact with a nearby CH? None of this kind of event has been reported ever. In this study, we present unambiguous evidence of such an event, revealing the collision between a set of coronal jets and a nearby CH with high quality data from the Atmospheric Imaging Assembly (AIA: Lemen et al. 2012) onboard the Solar Dynamics Observatory (SDO: Pesnell et al. 2012). It turns out that part of the jets is reflected towards the opposite direction, and this dynamical jet-CH interaction may have led to a successful eruption along the same direction.

2. Observations and Data Analysis

We mainly analyzed the AIA/SDO data that provides the essential observations of the event. The AIA instrument has ten EUV and UV wavelengths, covering a wide range of temperatures. The AIA observes the full disk (4096×4096 pixels) of the Sun and up to $0.5 R_{\odot}$ above the limb, with a pixel resolution of $0.6''$ and a cadence of 12 s. The eruption is visible in all AIA EUV channels. The passbands of interest here are 131 \AA (Fe XXI, ~ 10 MK), 211 \AA (Fe XIV, ~ 2.0 MK), 171 \AA (Fe IX, ~ 0.6 MK), and 304 \AA (He II, ~ 0.05 MK). Magnetograms and intensity maps from the Helioseismic and Magnetic Imager (HMI: Scherrer et al. 2012), with a cadence of 45 s and pixel

¹Note that during the peer-review process of our manuscript, a study reporting a CME event likely triggered by a coronal jet was published (Liu et al., 2015), which presents evidence supporting the close relation between a jet and a CME, with the jet pushing some overlying blob-like magnetic structure which later becomes the CME front and the jet likely evolves into the CME core.

scale of $0.6''$, were used to check the magnetic field configuration of the source region. The CME evolution in the high corona was captured by the Large Angle and Spectrometric Coronagraph (LASCO) C2 (Brueckner et al. 1995).

The kinematics of the jets and associated mass flow were analyzed with the time-slice approach. The speeds were determined by linear fits, with error bars given by the measurement uncertainty that is assumed to be 4 pixel (~ 1.74 Mm) for AIA data. We also used the Potential Field Source Surface (PFSS: Schrijver & De Rosa 2003) model to extrapolate the HMI photospheric field measurement to describe the large-scale magnetic field geometry.

3. Results

3.1. Coronal jets

The event occurred at the eastern boundary of the NOAA Active Region (AR) 12403 on 25 August 2015. Upper panels of Fig.1 show the AR image observed at AIA 211 Å, and the intensity map and magnetogram of HMI. The small white boxes (\sim S14E13) present the source area in which jets originated. It can be seen that the AR consists of a positive-polarity leading sunspot and a negative-polarity following sunspot. In the region given by white boxes, there exists a small parasitic positive polarity. An elongated low-latitude elephant-trunk CH exists eastward of the AR (white arrows in Fig.1a).

In Fig.1d-h, we present the sequence of HMI magnetogram from 03:30 UT to 11:30 UT to examine the magnetic evolution of the jet source region. As a result of earlier magnetic flux emergence, a small positive patch was embraced by negative dominant polarities and became the parasitic polarity. Comparing these magnetograms, we see that significant flux cancellation took place. This is further confirmed by the temporal changes of positive and negative magnetic fluxes in the FOV of Fig.1d-h, as plotted in Fig.1i. Before 07:12 UT (dashed vertical line), the negative flux increased continuously, while the positive counterpart did not change much. After 07:12 UT, both fluxes started to decrease with the positive one changing at a much steeper gradient. At about 10:20 UT (dotted vertical line), the positive flux presented an even faster declining rate.

The later time was consistent with the onset of the jet event. In the meantime, the GOES soft X-ray (SXR) profiles started to increase after 10:23 UT. Two SXR peaks were recorded in the following hour, corresponding to a C1.7 flare (peaking at 10:34 UT) and a C2.2 flare (peaking at 10:44 UT), respectively. Both flares were associated with jet activities. This is consistent with the general picture that jets are energized by magnetic reconnection, as evidenced here by significant flux cancellation and flare occurrence (e.g., Wang et al. 1998; Chae et al. 1999; Chifor et al. 2008; Yang et al. 2011; Liu et al. 2011; Pariat et al. 2009, 2015).

In Fig.2, we present the dynamical evolution of coronal jets observed at AIA 171 Å. As seen from Fig.2a-c and the accompanying animation, the jet started from the southern end of the

bright flaring loops, exhibiting a gradual footpoint migration towards the northern end. The migration indicates an apparent motion of the main flaring reconnection site. For the convenience of description, we separate the jets into three subsequent episodes, consisting of the initial relatively weak part (J1, starting at 10:26 UT), the middle part which is the strongest one and of particular interest to this study (J2, starting at 10:30 UT), and the third part which is basically confined by underlying loops (J3, starting at 10:38 UT). Note that similar confining mass flows have been used to trace the twisted structure internal of a flux rope (e.g., Li & Zhang 2013; Yang et al. 2014). These episodes of jets have been pointed out in Fig.2a-c. As mentioned, the jets mainly emanated from the FOV of Fig.1d-h, above the parasitic polarity. This is a general source property prescribed in jet modelling (e.g., Pariat et al. 2009, 2015). Because J1 was relatively weak and J3 was mostly confined, here we focus our study on J2.

Using the time-slice approach along the dotted line (S1) in Fig.2c, the derived velocity of J2 is close to 500 km s^{-1} (Fig.2f), much faster than the statistical average speed of $\sim 200 \text{ km s}^{-1}$ for jets (Shimojo et al. 1996). It is clear that J2 lasted for ~ 30 mins with continuous mass ejection. J2 initially moved along its associated AR loops, and carried the loops to extend. It is interesting to see that the forward extension of the jet-loop structure was suddenly stopped. The curved side of the jet-loop structure became flat-shaped with kinks at both ends, and part of J2 was clearly bounced towards the opposite direction while the left part returned to the solar surface (best seen in the online animation). The first sign of bounced-back material was present around 10:38 UT as seen from the online animation. The flat-shaped feature appeared around the interface between the nearby CH and the east edge of the AR, indicating that the jet carrying the loop ran into the AR-CH boundary and got reflected there. The reflection is also seen from the height-time plot along slices S2 and S3 (short lines in Fig.2d-e), from which we see a distinct V-type structure (Fig.2g-h). The speeds of the jet-loop structure along S2 and S3 before and after the reflection are nearly the same ($\sim 90 \text{ km s}^{-1}$).

Note that, after the jet-CH interaction, part of the jet material was stagnated (black arrows in Fig.2g-h) while the left part presented a signature of continuation of mass flows towards west (white arrows in Fig.2d-e, see also the online animation), at a fast speed of $\sim 400 \text{ km s}^{-1}$. See Fig.2i for the time-slice plot along S4. This is only slightly slower than the pre-collision jet. Yet, the jet front faded away shortly. So, it is not known, at this time, whether the reflected jet flows have escaped the corona or not.

3.2. CME and its relation with the jet

A weak CME feature appeared in the LASCO C2 FOV at 11:14 UT, with a hardly identifiable narrow front, developing into a much clearer CME structure in 10-20 mins (see Fig.3 and the accompanying animation). The central position angle of the ejecta at 11:26 UT was 238° (the angle increases counterclockwise with 0° along north). Initially, the CME presented a narrow jet-like morphology and later became diffusive without a clear flux-rope signature. It is thus difficult

to determine the exact type of this eruption (see Vourlidas et al. 2013). The appearance time of a clear CME signature in C2 is about 50 mins later than the first sign of the jet-CH collision ($\sim 10:38$ UT). In addition, the continuation part of the reflected jet flow is basically toward the CME direction. This close temporal-spatial correlation suggests that the jet may be associated with the CME.

It is crucial to further figure out whether the jet front continued its westward motion toward the solar limb to become a part of the CME or it actually moved downwards along a curved loop path and confined there. For short, we refer these suggestions to be the eruptive picture and the confining picture, respectively. In the following we present observational facts that, from our point of view, favor the first possibility.

Firstly, from Fig.4 and accompanying animations, in which a set of AIA images at 171, 211, and 131 Å are presented, we see that after 10:55 UT the jet front seemed to have moved beyond the associated AR loop system before its eventual fading-away, as pointed out by the arrows in Fig.4a-e, rather than returned to the solar surface along a curved loop-like path if being confined.

Secondly, following the jet front, since 11:06 UT a systematic westward motion of a set of loops started to appear, as pointed by arrows in Fig.4f-h, with a speed of $10\text{-}20 \text{ km s}^{-1}$. This is best seen from the online animations. The motion lasted for more than 30 mins, possibly an effect of continuous stretching exerted by the westward mass motion. Again, this is not inconsistent with the eruptive picture.

Thirdly, from the 304 Å data we observed an obvious outflow of filament-like dark material after 11:20 UT (see the white box in Fig.5a-c). It seems that the material corresponded to part of the reflected jet, being stagnated and accumulated around the jet-CH interaction region (best seen from the accompanying animation). They became dark possibly due to a cooling process. Note that there was no filament eruption observed during the event, so these dark material was not due to any filament eruption. Its outflow speed ($\sim 239 \text{ km s}^{-1}$) can be derived using the distance-time analysis along the slice S5 (Fig.5d). The 304 Å material moved out of the AR, along the direction pointing to the CME. This traces the open path from the jet-CH collision region to the CME, providing additional support to the first picture. Note that due to the time delay, the 304 Å material could not become the CME front yet they may provide some mass supply to the eruption.

The last observational fact worthy of mention is that no any other detectable eruptive activities were present on the solar disk according to all passband data of AIA, and on the back side according to the Extreme Ultraviolet Imager (EUVI) (Howard et al. 2008) on board the twin spacecraft of Solar-Terrestrial Relations Observatory (STEREO: Kaiser et al. 2008) with separation angles from the Earth 172.348° (STEREO-A) and 175.495° (STEREO-B) at the time.

In summary, the above observational facts favor the first picture, i.e., the post-collision jet further evolves into a part of the CME. The distance from the jet-CH interaction region to the CME front is $\sim 3 R_\odot$, indicating an average projected propagation speed of $\sim 700 \text{ km s}^{-1}$ if assuming the post-collision jet front later becoming the CME front. This is faster than the AIA-

measured projection speed of the jet, suggesting that either the jet gets further accelerated during its outward propagation or the jet is not the counterpart of the CME front and there exists other or earlier eruptive magnetic structures ahead of the jet. It should be pointed out that how the jet evolves into the CME and exactly which part of the CME corresponds to the jet front remains not resolved with available data set, partly due to the absence of CME signatures in the AIA FOV.

Further examining the PFSS results of the CH-AR magnetic field lines (Fig.3 c-d), we see that the CH open field lines are of negative polarity and lying next to the closed loop system that is rooted at the large negative polarity of the AR. The CH field lines, with a strong non-radial expansion, occupy the space above the closed AR loops. This magnetic configuration helps understand how the observed initially-collimated jet (along the eastern edge of the AR) runs into field lines of the nearby CH and then flows outward along the specific trajectory.

4. Summary

Here we present a first-of-its-kind observational study on a jet-CH colliding process showing that the post-collision jet was reflected towards the opposite direction. We also present compelling evidence supporting that the jet activity may have developed into a successful eruption (i.e., a CME). The jet-CH collision is evidenced by the flat morphology of the jet front observed by AIA, while the jet-CME relation is supported by their close temporal-spatial correlation, the observed outflow at 304 \AA , the large-scale CH-AR magnetic field configuration given by PFSS, and the fact that no other identifiable eruptive activities on the solar surface including the backside, among other observations. The presumed jet-CME route basically follows the over-expanding trend of the CH open field lines above the AR according to PFSS extrapolation, indicating a strong role played by the CH structure in defining the CME propagating direction. This is consistent with earlier studies, which were however not based on direct observation of CME-CH interaction, that CHs are important in affecting the CME propagating direction and thus the consequent geo-effectiveness. The study is possible because of the unprecedented high-quality data of AIA/SDO.

SDO is a mission of NASA's Living With a Star Program. The authors thank the SDO team for providing the data. This work is supported by grants NSBRSF 2012CB825601, NNSFC 41274175, and 41331068, and Yunnan Province Natural Science Foundation 2013FB085.

REFERENCES

- Brueckner, G. E., Howard, R. A., Koomen, M. J., Korendyke, C. M. et al. 1995, *Sol. Phys.*, 162, 357
- Chae, J., Qiu, J., Wang, H., & Goode, P. R. 1999, *ApJ*, 513, 75

- Chen, Y., Song, H. Q., Li, B., Xia, L. D. et al. 2010, *ApJ*, 714, 644
- Chen, H., Zhang J., & Ma, S. 2012, *Research in Astronomy and Astrophysics*, 12, 573
- Chifor, C., Isobe, H., Mason, H. E., Hannah, I. G., Young, P. R., Del Zanna, G., Krucker, S., Ichimoto, K., Katsukawa, Y., & Yokoyama, T. 2008, *A&A*, 491, 279
- Gopalswamy, N.; Mäkeä, P., Xie, H., Akiyama, S., & Yashiro, S. 2009, *Journal of Geophysical Research*, 114, A22
- Howard, R. A., Moses, J. D., Vourlidas, A., et al. 2008, *Space Sci. Rev.*, 136, 67
- Hundhausen, A. J., Holzer, T. E., & Low, B. C. 1987, *Journal of Geophysical Research*, 92, 11173
- Kaiser, M. L., Kucera, T. A., Davila, J. M., St. Cyr, O. C., Guhathakurta, M., & Christian, E. 2008, *Space Sci. Rev.*, 136, 5
- Lemen, James R., Title, Alan M., Akin, David J., Boerner, Paul F. et al. 2012, *Sol. Phys.*, 275, 17
- Li, T., & Zhang, J. 2013, *ApJ*, 770, L25
- Liu, C., Deng, N., Liu, R., Ugarte-Urra, I., Wang, S., & Wang, H. 2011, *ApJ*, 735, L18
- Liu, J., Wang, Y., Shen, C., Liu, K., Pan, Z., & Wang, S. 2015, *ApJ*, 813, 115
- Pariat, E., Antiochos, S. K., & DeVore, C. R. 2009, *ApJ*, 691, 61
- Pariat, E., Dalmasse, K., DeVore, C. R., Antiochos, S. K., & Karpen, J. T. 2015, *A&A*, 573, 130
- Pesnell, W. Dean, Thompson, B. J., Chamberlin, P. C. et al. 2012, *Sol. Phys.*, 275, 3
- Rachmeler, L. A., Pariat, E., DeForest, C. E., Antiochos, S. K., & Török, T. 2010, *ApJ*, 715, 1556
- Savcheva, A., Cirtain, J., Deluca, E. E. et al. 2007, *Publications of the Astronomical Society of Japan*, 59, 771
- Scherrer, P. H., Schou, J., Bush, R. I., Kosovichev, A. G., et al. 2012, *Sol. Phys.*, 275, 207
- Schmieder, B, Shibata, K., van Driel-Gesztelyi, L., & Freeland, S. 1995, *Sol. Phys.*, 156, 245
- Schrijver, Carolus J., & De Rosa, Marc L. 2003, *Sol. Phys.*, 212, 165
- Sheeley, N. R., Hakala, W. N., & Wang, Y. -M. 2000, *Journal of Geophysical Research*, 105, 5081
- Shibata, K, Ishido, Y., Acton, L. W. et al. 1992, *Publications of the Astronomical Society of Japan*, 44, 173
- Shibata, K, Nakamura, T, Matsumoto, T. et al. 2007, *Science*, 318, 1591

- Shimojo, M., Hashimoto, S., Shibata, K., Hirayama, T., Hudson, Hugh S. & Acton, L. W. 1996, Publications of the Astronomical Society of Japan, 48, 123
- Tripathi, D., & Raouafi, N. -E. 2007, A&A, 473, 951
- Tsuneta, S., Acton, L., Bruner, M., Lemen, J. et al. 1991, Sol. Phys., 136, 37
- Vourlidas, A., Lynch, B. J., Howard, R. A., & Li, Y. 2013, Sol. Phys., 284, 179
- Wang, H., Johannesson, A., Stage, M., Lee, C., & Zirin, H. 1998, Sol. Phys., 178, 55
- Yang, S., Zhang, J., Li, T., & Liu, Y. 2011, ApJ, 732, L7
- Yang, S., Zhang, J., Li, T., Liu, Z., & Xiang, Y. 2014, ApJ, 784, L36

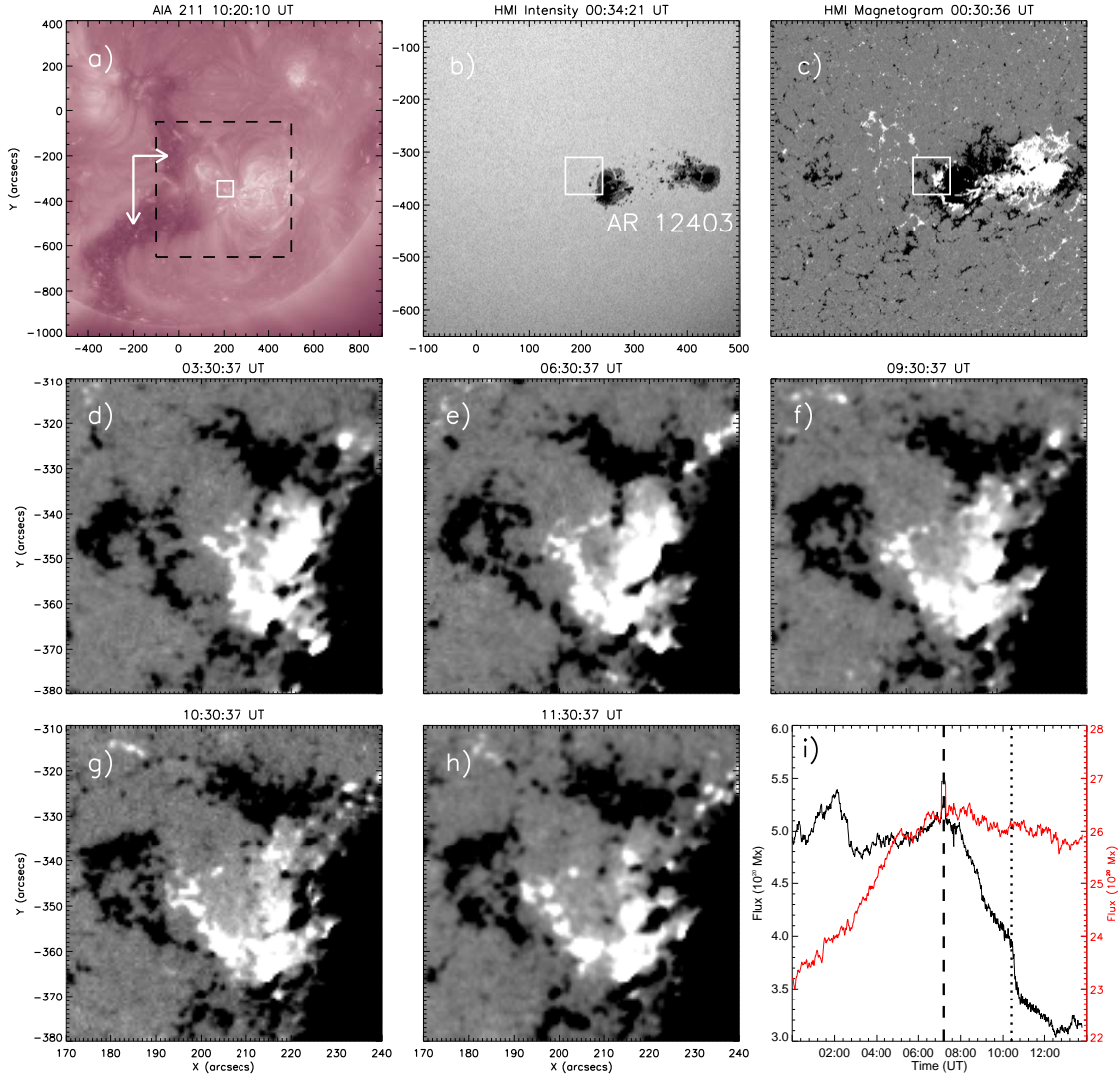


Fig. 1.— Overview of the NOAA AR 12043 and the magnetic evolution of the event. (a) AIA 211 Å image showing the eruption region (white box) and the adjacent “elephant trunk” CH (white arrows), in which the black box indicates the FOV of (b-c). (b-c) HMI intensity map and HMI magnetogram showing the eruption region (white box) and the AR. (d-h) A sequence of HMI magnetograms showing the magnetic cancellation regions, in a FOV indicated by the box in panel c. (i) The changes of the negative (red) and positive (black) magnetic fluxes within the FOV of panels (d-h). The vertical dashed and dotted lines mark the onset of the abrupt decreasing and the beginning of the eruption, respectively. A color figure is available online.

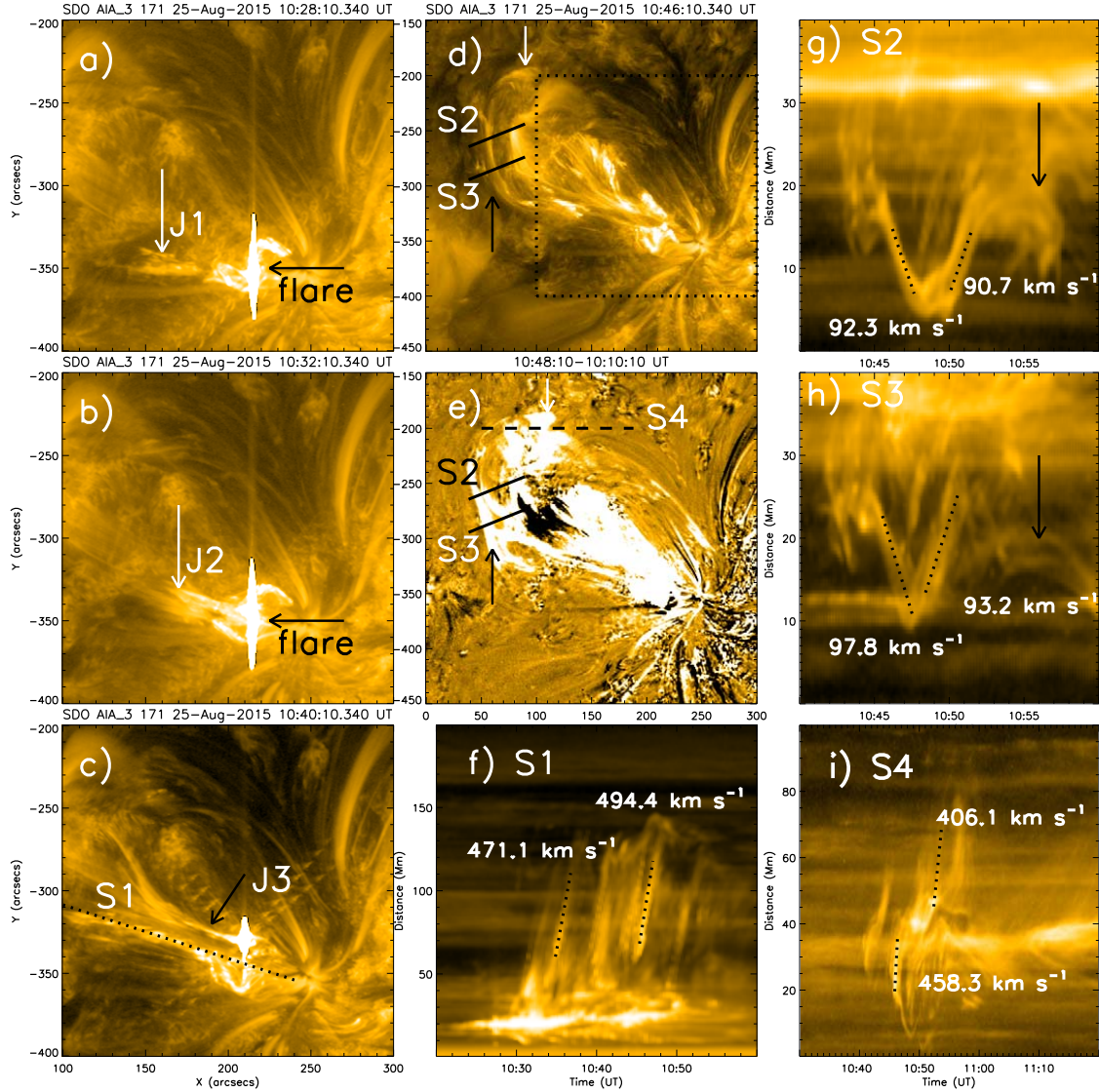


Fig. 2.— Coronal jets and their interaction with the nearby CH, observed at AIA 171 Å. (a-c) Images showing the coronal jets (J1-J3) and the associated flaring loops. (d-e) Images showing the jet-CH interaction. The short lines (S2-S3) are used to construct slice-time plots revealing the deflection of the jet-loop structure. The black dashed box in (d) indicates the FOV of (a-c). (f) Slice-time plot showing the motion of the J2 along S1. (g-h) Slice-time plots along slices S2-S3. The flow stagnation is pointed out by black arrows. (i) Slice-time plot along S4. The dotted lines are used to derive the linearly-fitted speeds. A color figure and an accompanying animation are available online.

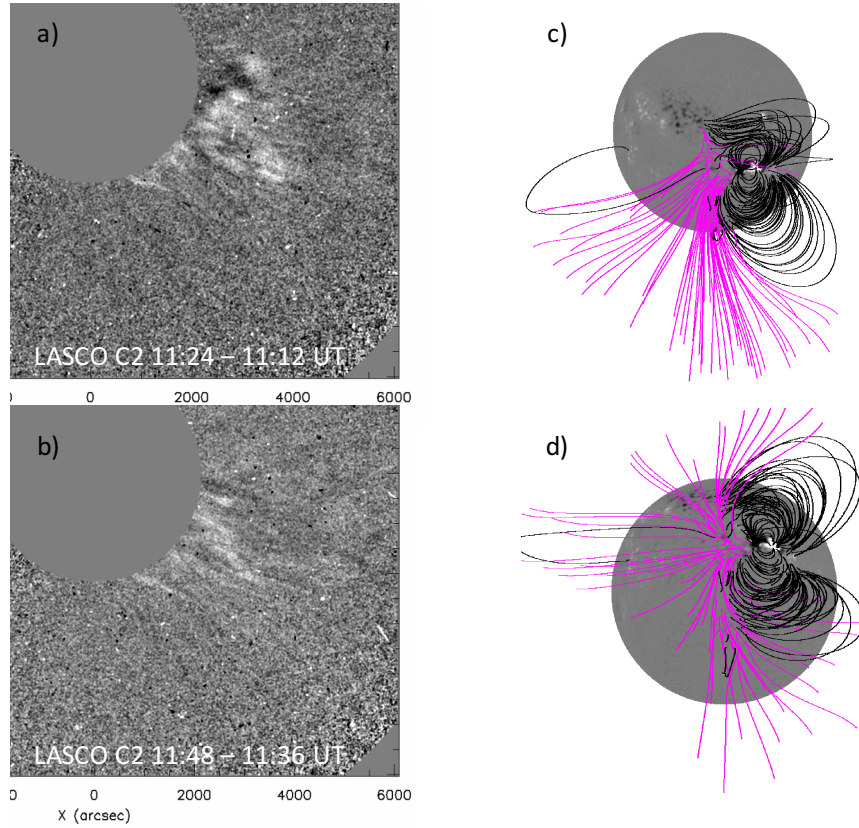


Fig. 3.— CME evolution and PFSS extrapolation results. (a-b) LASCO C2 images of the CME. (c-d) PFSS extrapolated field lines for the CH open field lines (purple) and the active region closed field lines (black). Panel (c) corresponds to the AIA FOV, while panel (d) is given by an upward (northward) rotation of panel (c) by 50° , to show up more details of the over expansion of the CH magnetic field lines. A color figure and an accompanying animation are available online.

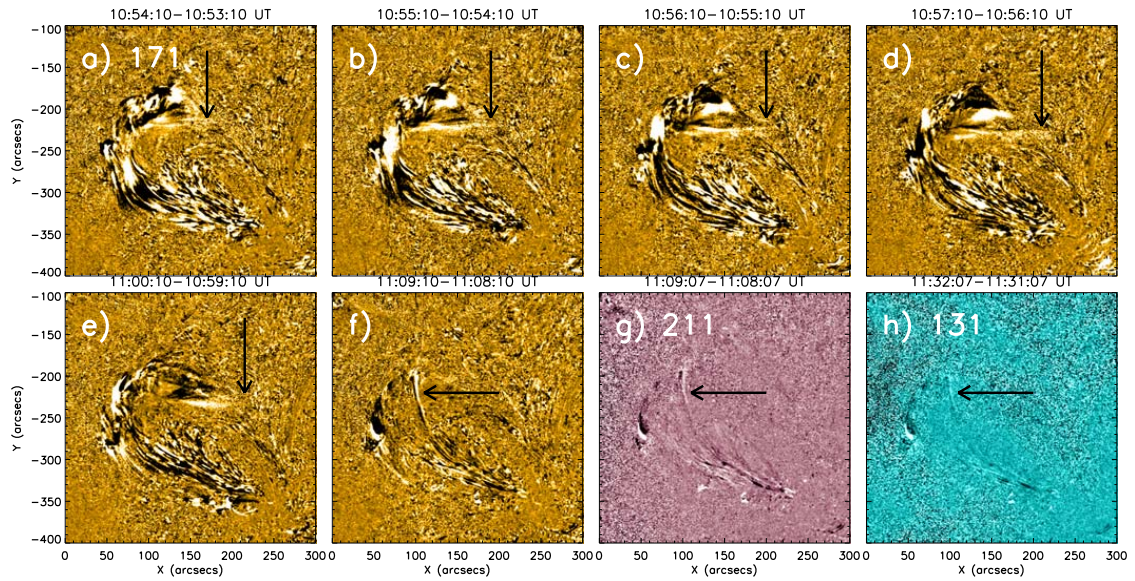


Fig. 4.— AIA images at 171 (a-d), 211 (e-f), and 131 Å (g-h) highlighting the continuation of the jet mass flow towards west and the associated post-jet motion. Arrows in (a-d) point to the fast westward-moving jet fronts, and arrows in (e-h) point to the relatively slow westward-moving loops. A color figure and 3 accompanying animations are available online.

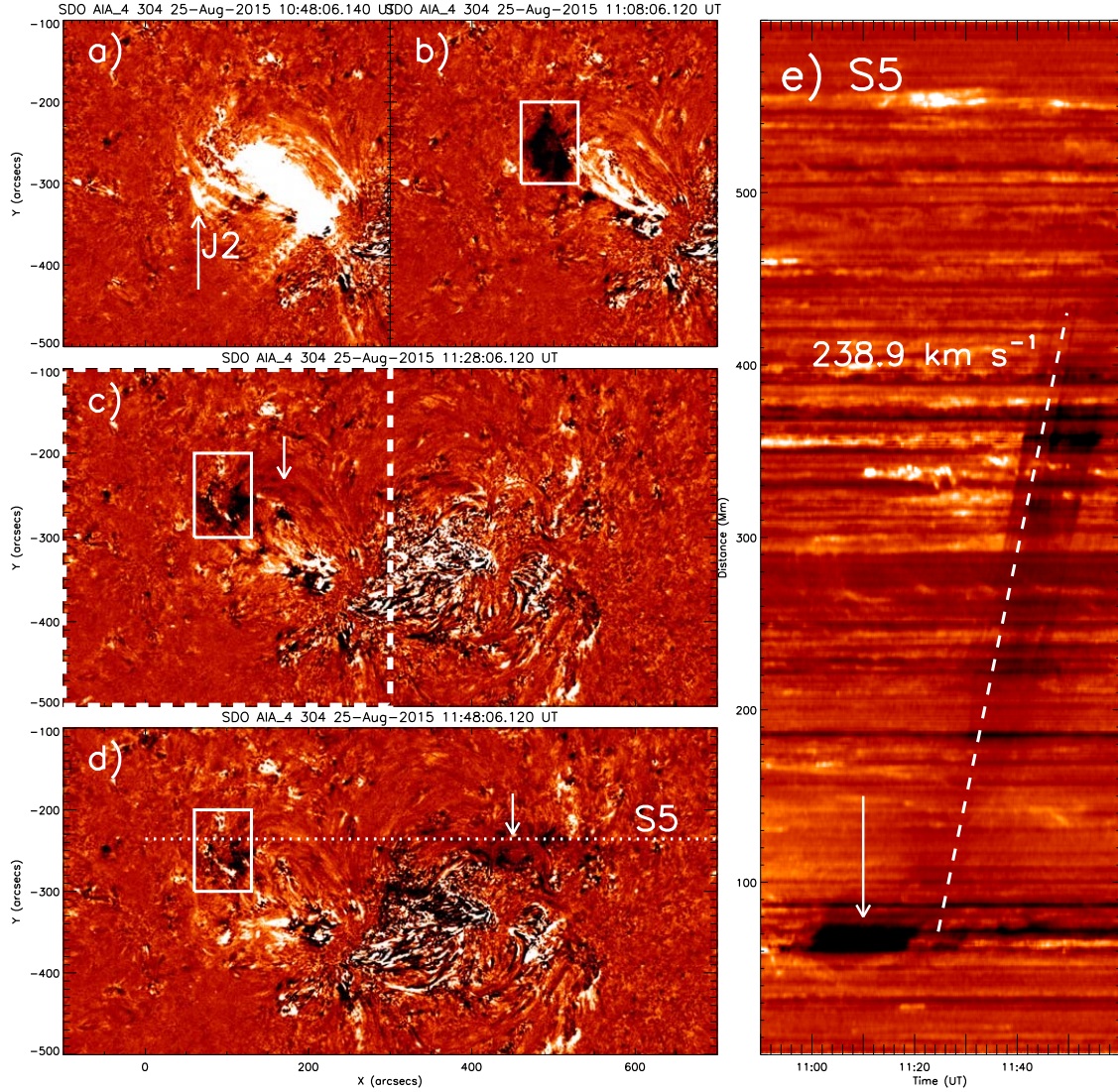


Fig. 5.— Accumulation and drift of the dark filament-like mass observed at AIA 304 Å. (a-b) Base-difference images exhibiting the accumulation of the jet mass as indicated by the white box. (c-d) Base-difference images illustrating the drift of the 304 Å material (white arrows). The dotted line in panel (d) is selected to construct a slice-time plot displaying the mass flow. The dashed box in panel (c) indicates the FOV of panels (a-b). (e) Slice-time plot along the slice S5. The dashed line is used to obtain the speed of mass flow. A color figure and an accompanying animation are available online.